

LEDCNet: A Lightweight and Efficient Semantic Segmentation Algorithm Using Dual Context Module for Extracting Ground Objects from UAV Aerial Remote Sensing Images

Xiaoxiang Han, Yiman Liu, Gang Liu, Qiaohong Liu

Abstract—Semantic segmentation of UAV aerial remote sensing images provides a more efficient and convenient surveying and mapping method for traditional surveying and mapping. In recent years, convolution-based semantic segmentation neural networks have evolved to become larger and more complex. In addition, with the rise of Transformer, it quickly replaced the convolutional neural network and became the most advanced model in the field of computer vision. However, recently, the number of parameters of the semantic segmentation model has become larger and larger, and the complexity has become higher and higher. This is obviously not conducive to the wide application of the model in the industry. In order to make the model lightweight and improve a certain accuracy, this research developed a new lightweight and efficient network for the extraction of ground features from UAV aerial remote sensing images, called LDMCNet. Meanwhile, this research develops a powerful lightweight backbone network for the proposed semantic segmentation model. It is called LDCNet, and it is hoped that it can become the backbone network of a new generation of lightweight semantic segmentation algorithms. The proposed model uses dual multi-scale context modules, namely the Atrous Space Pyramid Pooling module (ASPP) and the Object Context Representation module (OCR). In addition, this research constructs a private dataset for semantic segmentation of aerial remote sensing images from drones. This data set contains 2431 training sets, 945 validation sets, and 475 test sets. The proposed model performs well on this dataset, with only 1.4M parameters and 5.48G floating-point operations (FLOPs), achieving an average intersection-over-union ratio (mIoU) of 71.12%. 7.88% higher than the baseline model. In order to verify the effectiveness of the proposed model, training on the public datasets "LoveDA" and "CITY-OSM" also achieved excellent results, achieving mIoU of 65.27% and 74.39%, respectively. The source code is available at <https://github.com/GtLinyer/LEDCNet>.

Index Terms—Remote Sensing, Semantic Segmentation, Context Features, Lightweight Network

I. INTRODUCTION

THE application of remote sensing images taken by unmanned aerial vehicles (UAVs) is of great significance. Compared with other aerial photography collection methods, drones have certain advantages in land surveying and mapping. It is less susceptible to atmospheric interference, has a low flight altitude, high resolution and, above all, low operating costs [1].

In recent years, with the continuous development of deep learning, models based on convolutional neural networks have shown excellent results in multiple tasks such as image classification, detection, and segmentation. Compared with traditional algorithms, deep learning can automatically extract features without manually extracting features from the color, texture, shape and spatial position relationship of the image. In the task of semantic segmentation of natural images, since the introduction of the Fully Convolutional Network (FCN) [2], there have been many excellent works that have significantly improved the performance of the semantic segmentation model [3]–[9]. These algorithms predict pixel-level labels based on the semantic information represented by image pixels.

Different from natural images, UAV aerial remote sensing images are often very large in size, usually with a resolution of tens of thousands by tens of thousands. In terms of image content, even the same type of ground features may have large differences. For example, some buildings have different styles. However, some different types of surface feature elements may be similar. For example, the top of a concrete building is very similar to the surface of a concrete road. Some surface feature elements may be very complex and difficult to extract. For example, there are often many vehicles on the road. There will be a lot of greenery on both sides or in the center of the road, and the vegetation in it will block the road. In addition, buildings with different scales are likely to affect the performance of the model, as shown in Fig.1. Therefore, this requires the model to have a strong ability to extract multi-scale context features.

To address these issues, a new deep neural network structure, called **Lightweight and Efficient Network** implemented Using **Dual Context** modules (LEDCNet), is proposed for the

This research was partially supported by the National Natural Science Foundation of China (Project No. 61801288).

Xiaoxiang Han and Yiman Liu are equally contributed, and Qiaohong Liu is the corresponding author.

Xiaoxiang Han is with the School of Health Sciences and Engineering, University of Shanghai for Science and Technology, Shanghai 200093, China (e-mail: gtlinyer@163.com).

Yiman Liu is with Department of Pediatric Cardiology, Shanghai Children's Medical Center, School of Medicine, Shanghai Jiao tong University, Shanghai 200127, China, and Shanghai Key Laboratory of Multidimensional Information Processing, School of Communication & Electronic Engineering, East China Normal University, Shanghai 200241, China (e-mail: Liuyiman-SCMC@163.com).

Gang Liu is with the Key Laboratory of Earthquake Geodesy, Institute of Seismology, China Earthquake Administration, Wuhan 430071, China (e-mail: whgpslg@gmail.com).

Qiaohong Liu is with the School of Medical Instruments, Shanghai University of Medicine and Health Sciences, Shanghai 201318, China (e-mail: hqlq@163.com).

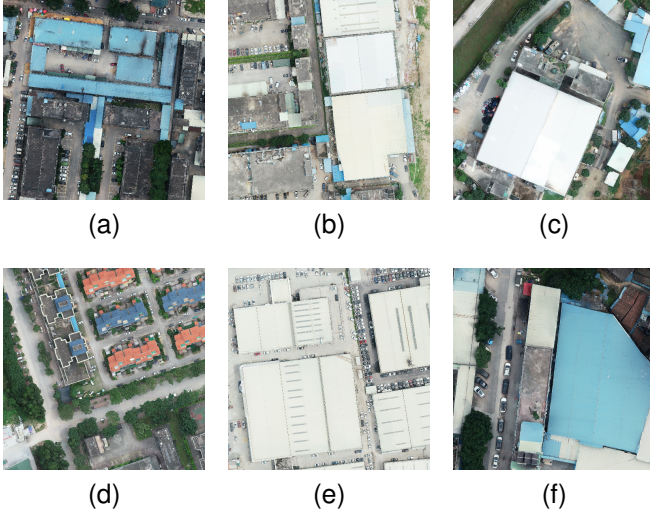


Fig. 1. Some examples of features from our private dataset. The styles of the different buildings in (a) and (d) are quite different. Concrete building roofs and concrete pavements in (b) and (e) are very similar. (c) and (f) have buildings of various sizes. The roads in these images have vehicles and are occluded by vegetation.

extraction of ground features from UAV aerial remote sensing images. The proposed model is an encoder-decoder structure. There are dual context feature extraction modules in the decoder module, which are the Atrous Spatial Pyramid Pooling (ASPP) module [8] and the Object Context Representation (OCR) module [10]. After ASPP, the Feature Pyramid Network (FPN) module [11] is used to fuse multi-scale features.

In our research practice, we found that DenseNet [12] has a strong feature extraction ability, but its parameters and calculations are large. Moreover, Liu et al. [13] developed a convolutional neural network called ConvNeXt. They obtained a powerful convolutional neural network beyond Swin Transformer [14] by improving ResNet [15]. Inspired by this, this research develops a lightweight high-performance convolutional neural network based on their ideas. It is called **Lightweight Densely Connected Network (LDCNet)**. And using LDCNet as the backbone network of the proposed model for semantic segmentation of remote sensing images has achieved excellent results. The main contributions of this paper are as follows.

- 1) This research develops a network of encoder-decoder structure for the extraction of feature elements from UAV aerial remote sensing images, which has a dual multi-scale contextual feature extraction module.
- 2) This research uses the design ideas of ConvNeXt and DenseNet to develop a lightweight and high-performance backbone network.
- 3) This research comprehensively compares the effect of several most popular backbone networks and semantic segmentation algorithms on semantic segmentation of UAV aerial remote sensing images. And further visualize and analyze the features of its output feature map. Secondly, the efficiency of each algorithm is analyzed.

II. RELATED WORKS

A. Semantic Segmentation in Remote Sensing

With the birth of FCN, the originator of semantic segmentation network based on deep learning, it was soon applied to the field of remote sensing. However, compared with natural images, remote sensing images are much more complex, and FCN cannot be directly applied to remote sensing image semantic segmentation. For the first time, Maggiori et al. [16] adopted a deep learning-based method for semantic segmentation of remote sensing images. They designed a dual-scale neuron module based on FCN, which balances the accuracy of recognition and localization. Liu et al. [17] applied their improved FCN to high-resolution aerial remote sensing image segmentation. But FCN has limited ability to extract objects of very small size or very large size [2]. Fu et al. [18] adopted dilated Atrous convolution to optimize the FCN model and used conditional random field (CRF) to post-process the segmented data. Their segmentation accuracy improves significantly over previous networks. Atrous convolution can increase the receptive field of the convolution while maintaining the spatial resolution of the feature map.

U-Net [4] is another flow-type semantic segmentation network, which was first used in medical image segmentation. Li et al. [19] proposed a network for land and sea segmentation of high-resolution remote sensing images based on U-Net. In addition, Cheng et al. [20] proposed a network called HDCUNet combining U-Net with Hybrid Dilated Convolution (HDC) for fast and accurate extraction of coastal farming areas. It avoids meshing and increases the receptive field. Wang et al. [21] designed a U-Net with two decoders and introduced spatial attention and channel attention.

In addition, researchers [3], [22] have improved SegNet [3] for semantic segmentation of remote sensing images. Weng et al. [23] proposed an SR-SegNet using a separable residual algorithm for water extraction from remote sensing images. Kniaz et al. [24] developed a network called GeoGAN based on the Generative Adversarial Network (GAN) [25] to extract waters in different seasons. In addition, some researchers [26]–[28] have improved the semantic segmentation model based on Transformer or the combination of Transformer and CNN. Although Transformer has a global receptive field, its inherent defect is that the amount of calculation is too large.

B. Lightweight Network

In order to enable models to run on devices with limited resources (such as drones for remote sensing aerial imaging), it is necessary to design lightweight and efficient networks. The MobileNet series [29]–[31] is a classic lightweight network that applies depthwise separable convolutions [29], inverted residuals [30], linear bottlenecks [30], and lightweight channel attention modules [31]. It can achieve higher accuracy with lower parameter amount and calculation amount. In addition, the lightweight network has SqueezeNet [32], which uses the Fire module for parameter compression. EffectionNett [33] balances the three dimensions of depth, width, and resolution well, and scales these three dimensions uniformly through a set of fixed scaling factors. GhostNet [34] obtains redundant

information by designing cost-efficient, which ensures that the model fully understands the input data. MicroNet [35] uses Micro-Factorized convolution and Dynamic Shift-Max two designs to reduce the amount of calculation and improve network performance.

C. Context Feature Extraction

In order to solve the problem of receptive field scale, the semantic segmentation network needs to fully consider the context information. PSPNet [5] uses a pyramid pooling module, which connects four global pooling layers of different sizes in parallel, pools the original feature maps to generate feature maps of different levels, and restores them to the original size after convolution and upsampling. Through this operation it is possible to aggregate multi-scale contextual features. DeepLabV3 [8] uses the Atrous spatial pyramid pooling (ASPP) module, which uses different hole rates to construct convolution kernels of different receptive fields to obtain multi-scale context information. Cao et al. [36] proposed GCNet, which uses a self-attention mechanism to obtain global context information. Peng et al. [37] proposed GCN. They increased the receptive field by increasing the size of the convolution kernel. They even designed a convolution kernel up to 15×15 in size, which proved that the large convolution kernel has a stronger ability to extract context features.

III. PROPOSED METHOD

A. Overall structure of LEDCNet

The proposed LEDCNet is an encoder-decoder structure whose backbone network is the proposed LDCNet. Its input is a picture of size 512×512 . First, the backbone network takes four different levels of feature maps as output. The first three feature maps are respectively input into the Atrous spatial pyramid pooling module (ASPP) [8] to extract multi-scale context information. These feature maps are respectively processed by the Feature Pyramid Network (FPN) [11] and then upsampled to the same size. These feature maps of the same size are then concatenated. Then input the feature map into an Object-Contextual Representation (OCR) [10] module to obtain the context relationship of pixels of the same category. Finally, the feature maps are processed by a refinement classification head to refine the segmentation edges. The overall architecture of LEDCNet and the details of ASPP are shown in Fig.2.

B. LDCNet

Inspired by ConvNeXt and DenseNet, this research develops a backbone network called LDCNet. Its overall structure and densely connected blocks are shown in Fig.4. The authors of ConvNeXt designed a series of design decisions, summarized as: macro design, reference of ResNeXt's design ideas [38], inverted bottleneck layer, large convolution kernel and micro design of various layers.

In terms of macro design, the stacking ratio of ConvNeXt's 4-stage blocks is 1:1:3:1. That is, the number of blocks stacked in the third stage is larger. Furthermore, researchers have

thoroughly studied the distribution of computation [39], [40]. Like ConvNeXt, we set the stacking ratio of the 4-stage blocks of LDCNet to 1:1:3:1. The specific layers of each stage are 8, 8, 24 and 8 respectively. Its overall structure is shown in Fig.3.

ConvNeXt designs an inverted bottleneck layer (Fig.4(a).) and lifts 3×3 convolutions to the beginning (Fig.4(b).). Also, this 3×3 convolution is a depthwise separable convolution. This structure can partially reduce the parameter scale of the model and improve the overall performance of the model while slightly improving the accuracy rate. In addition, in order to enable the model to obtain the ability of multi-scale feature extraction, this study draws on the multi-branch idea of Inception in GooLeNet [41] and designs two branches. One of the branches is a depthwise separable convolution with a 7×7 size convolution kernel, and the other is a depthwise separable convolution with a 3×3 size convolution kernel. Then add their output feature maps, and finally concatenate with the input feature map of the bottleneck layer as the output feature map of the bottleneck layer (Fig.4(c).).

In the past period of time, CNN has used a large convolution kernel, such as AlexNet [42], which has used a convolution kernel as large as 11×11 . But as VGGNet [43] generalizes the gold standard 3×3 size convolution kernel, this stack of small kernel size convolution layers has efficient hardware implementation on modern GPUs [44]. In recent years, some new studies [37], [45], [46] have shown that large convolution kernels are more efficient for improving the receptive field. In order to have higher computational efficiency, we choose a convolution kernel with a size of 7×7 . We place this large convolutional kernel at the beginning of a branch of the bottleneck layer.

Batch normalization (BN) [47] is a way to make neural network training faster and more stable. It computes the mean and variance of each minibatch and pulls it back to a standard normal distribution with mean 0 and variance 1. However, it may have drawbacks that are detrimental to the model [48]. BN is still preferred in most current computer vision tasks. However, what is used in Transformers is simple layer normalization (layer normalization, LN) [49]. It is more common in natural language processing tasks. ConvNeXt replaces all BNs with LNs. Their experiments show that doing so can improve the performance of the model. However, we believe that it is inappropriate to do so in the task of extracting ground features from UAV aerial remote sensing images. Because, the features of our remote sensing images depend on the statistical parameters between different samples. Therefore, we only replace part of BN in LDCNet. Specifically, we use an LN after a 3×3 depthwise separable convolution in the bottleneck layer. In addition, we replaced the BN in the transition layer with LN.

C. Atrous Space Pyramid Pooling (ASPP)

In order to obtain a large receptive field without losing spatial resolution and without increasing computation, ASPP uses multiple parallel dilated convolutional layers with different sampling rates. The features they extract for each sampling

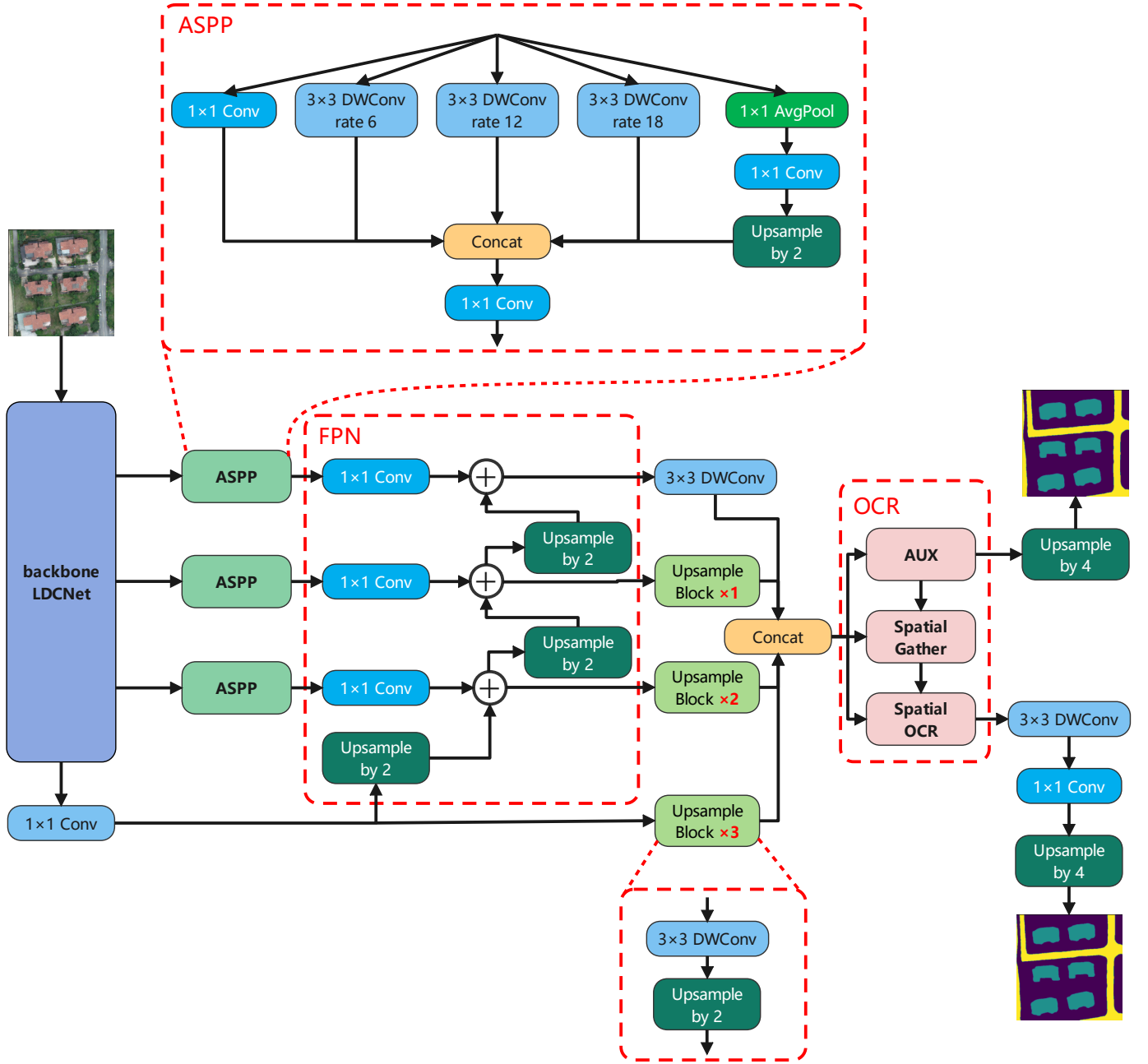


Fig. 2. The overall architecture of LEDCNet, and the details of ASPP.

rate are further processed in separate branches and fused to generate the final result. Atrous convolution can expand the receptive field of the convolution kernel without loss of resolution. Using ASPP can achieve multi-scale feature extraction through different receptive fields and upsampling. In a two-dimensional convolution, for each position i on the feature y of the convolution output and the corresponding convolution kernel w , for the input x , the calculation of the dilated convolution is as follows:

$$y[i] = \sum_k x[i + r \cdot k]w[k] \quad (1)$$

Where r is the hole rate, which represents the sampling step size of the convolution kernel on the input x of the convolution

operation. k represents the position of the convolution kernel parameter. If the convolution kernel size is 3, then $k=0,1,2$. The receptive field of the convolution can be adaptively modified by changing the value of the dilation rate r .

D. Object Context Representation (OCR)

OCR considers the relationship between a loxel and its context loxels, and aggregates similar context loxel representations with higher weights. Unlike relational context methods. OCR constructs contextual pixels into object regions and exploits the relationship between pixels and object regions.

The OCR module consists of three steps: soft object region extraction, object region representation computation, and

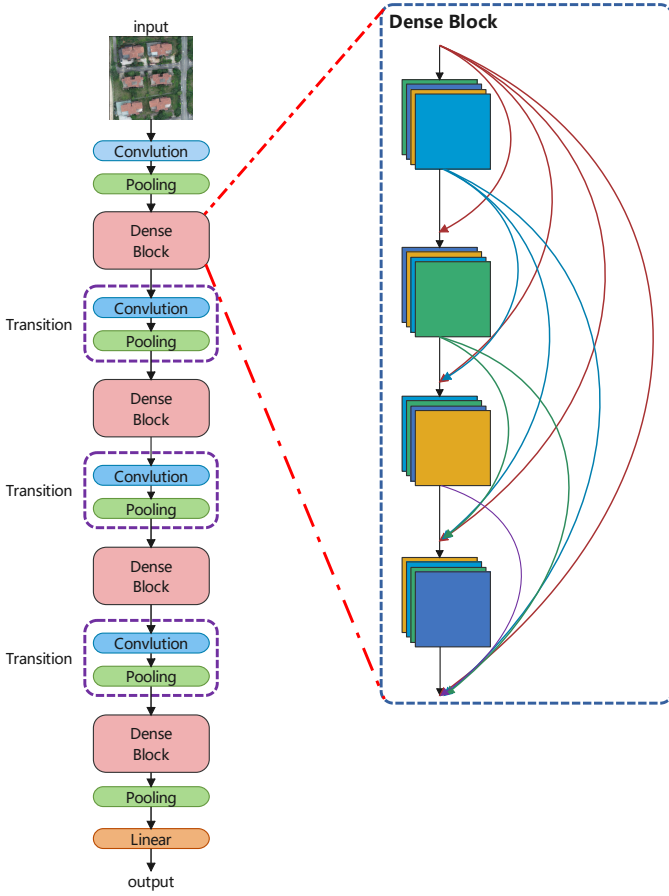


Fig. 3. The overall structure and densely connected blocks of LDCNet.

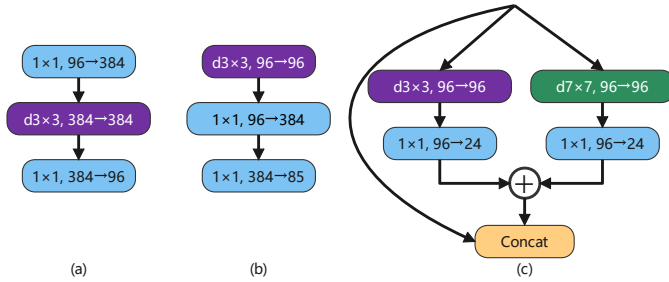


Fig. 4. (a) is the inverted bottleneck layer designed by the authors of ConvNeXt. (b) is the bottleneck layer of ConvNeXt. (c) is our bottleneck layer for LDCNet.

object-contextual representation computation for each position. It is mainly based on the scaled dot-product self-attention of the encoder-decoder structure. The input to attention consists of: a set of N_q queries $Q \in \mathbb{R}^{d \times N_q}$, a set of N_{kv} keys $K \in \mathbb{R}^{d \times N_{kv}}$, and a set of N_{kv} values $V \in \mathbb{R}^{d \times N_{kv}}$. The attention weight a_j is computed as the Softmax normalization of the dot product between query q_i and key k_j :

$$Z_i = \sum_{j=1}^{N_{kv}} e^{\frac{1}{\sqrt{d}} q_i^\top k_j} \quad (2)$$

$$a_{ij} = \frac{e^{\frac{1}{\sqrt{d}} q_i^\top k_j}}{Z_i} \quad (3)$$

The attention output for each query q_i is the aggregation of values weighted by attention weights:

$$\text{Attn}(q_i, K, V) = \sum_{j=1}^{N_{kv}} a_{ij} V_j \quad (4)$$

For object context representation, the calculation formula of the relationship between each pixel and each object area is as follows:

$$w_{ik} = \frac{e^{\kappa(x_i, f_k)}}{\sum_{j=1}^K e^{\kappa(x_i, f_j)}} \quad (5)$$

Among them, $\kappa(x, f) = \phi(x)^\top \psi(f)$ is the denormalized relationship function, $\phi(\cdot)$ and $\psi(\cdot)$ are two transformation functions implemented by $1 \times 1 \text{Conv} \rightarrow \text{BN} \rightarrow \text{ReLU}$.

IV. EXPERIMENT

A. Dataset

We constructed a private dataset of aerial remote sensing images taken by drones, including 2431 images in the training set, 945 images in the verification set, and 676 images in the test set. Our dataset contains two types of ground features, buildings and roads. The training and validation sets are from a city in Guangdong, China, and the test set is from a place along the Yangtze River. Furthermore, in order to verify the competitive performance and model generalization ability of our proposed model in the task of semantic segmentation of aerial remote sensing images, we test it on two public datasets "LoveDA" [50] and "CITY-OSM" [51]. "LoveDA" includes the cities of Nanjing, Changzhou and Wuhan in China, with a total of 5987 high spatial resolution (0.3 m) remote sensing images. It has 2522 training sets, 1669 validation sets, and 1796 test sets. This dataset originally has 6 types of ground features, but for the sake of fairness, we only take two types of ground features, buildings and roads. "CITY-OSM" includes Berlin and Potsdam in Germany, Chicago in the United States, Paris in France, Zurich in Switzerland and Tokyo in Japan, with a total of 1641 aerial images. Its labels are two types of ground features, houses and roads, which are consistent with the label categories of our private dataset. We remove obviously mislabeled images in this dataset (such as labeling the entire image as a house or a road), and crop and scale the image to 512×512 . Then we divide it into a training set of 10621 images, and a validation set and a test set of 3401 images.

B. Training Details

We designed our model based on the machine learning framework PyTorch1.12.1 using Python3.8. In particular, we also use PyTorch-Lightning1.6.5, an efficient and convenient framework based on PyTorch. In addition, some of our comparison experiments and ablation experiments use the backbone network provided in Torchvision0.13.1.

We train the model on a GPU server. This server contains 1 CPU (Intel Core i9-10900X), a total of 32GB of RAM, 2 GPUs (Nvidia RTX3080 10GB), a total of 20GB of VRAM.

TABLE I
EXPERIMENTAL RESULTS ON THE PRIVATE DATASET.

Method	Backbone	Background (%)	house (%)	road (%)	OA (%)	mean F1 (%)	mIoU (%)
DC-Swin	-	76.47	55.74	23.17	87.08	65.44	52.14
SegFormer	-	78.55	56.94	36.23	88.37	71.24	57.24
GCNet	ResNet18	79.55	61.53	37.72	89.09	73.19	59.62
A2FPN	ResNet18	81.46	66.01	41.73	90.33	76.06	63.26
PSPNet	ResNet18	82.56	67.52	43.87	90.89	76.92	64.22
BuildFormer	-	83.26	68.56	47.76	91.34	78.95	66.53
LEDCNet (ours)	LDCNet (ours)	85.73	75.01	52.70	92.83	82.35	71.12

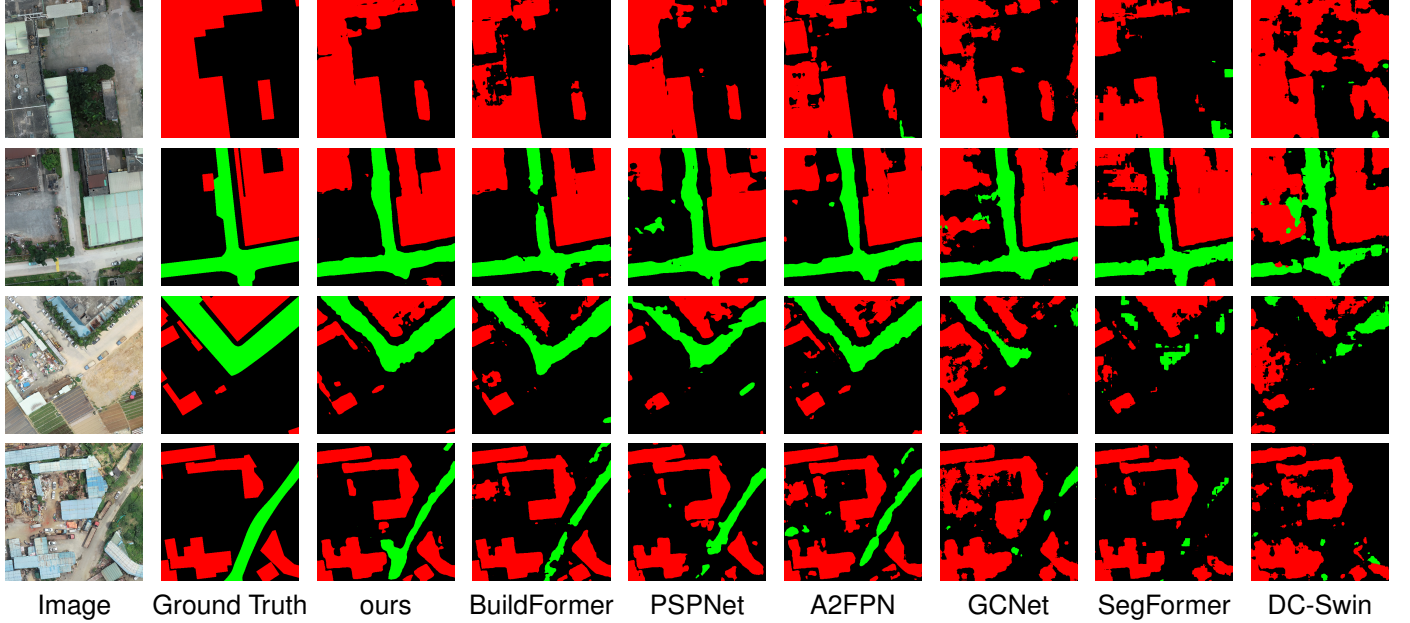


Fig. 5. Experimental results on the private dataset.

TABLE II
EXPERIMENTAL RESULTS ON THE PUBLIC DATASET "LOVEDA"

Method	Backbone	Background (%)	house (%)	road (%)	OA (%)	mean F1 (%)	mIoU (%)
DC-Swin	-	88.41	32.94	24.34	92.47	60.85	48.57
SegFormer	-	90.85	36.00	33.89	93.60	66.10	53.31
GCNet	ResNet18	89.83	37.02	35.04	93.56	66.85	53.90
A2FPN	ResNet18	90.18	38.82	43.59	93.82	70.49	57.59
PSPNet	ResNet18	91.07	48.55	44.05	94.81	74.05	61.43
BuildFormer	-	91.94	49.97	50.26	94.97	76.44	64.05
LEDCNet (ours)	LDCNet (ours)	92.65	54.01	49.13	95.42	77.41	65.27

TABLE III
EXPERIMENTAL RESULTS ON THE PUBLIC DATASET "CITY-OSM"

Method	Backbone	Background (%)	house (%)	road (%)	OA (%)	mean F1 (%)	mIoU (%)
DC-Swin	-	63.71	68.79	55.06	85.42	76.79	62.52
SegFormer	-	67.35	72.69	61.73	87.48	80.34	67.26
GCNet	ResNet18	66.67	71.76	63.44	87.32	80.39	67.28
A2FPN	ResNet18	71.12	75.72	77.65	89.26	83.34	71.50
PSPNet	ResNet18	75.40	79.01	73.10	91.06	86.24	76.04
BuildFormer	-	75.36	79.30	72.79	91.08	86.22	75.82
LEDCNet (ours)	LDCNet (ours)	73.95	78.25	70.95	90.49	85.28	74.39
LEDCNet-Large (ours)	LDCNet-large (ours)	75.51	79.51	73.30	91.17	86.41	76.10

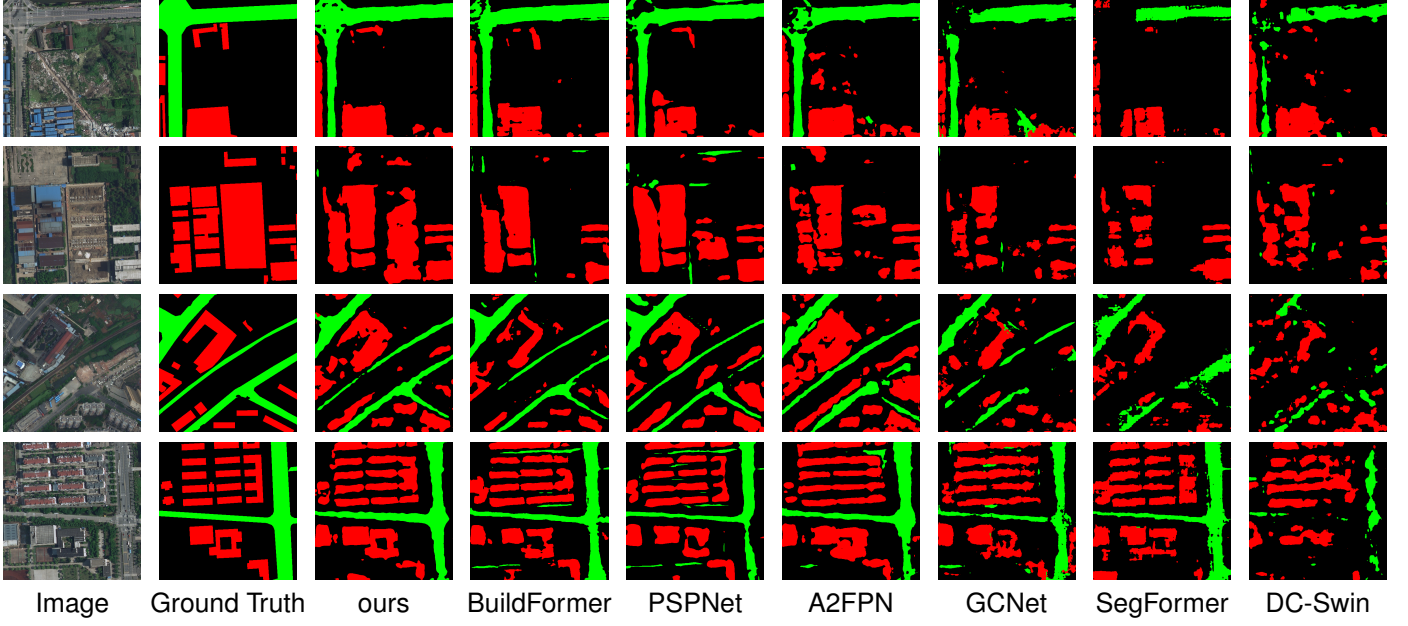


Fig. 6. Experimental results on the public dataset "LoveDA".

Main parameter settings: Set the batch size of data according to different networks to ensure maximum memory utilization. The number of threads of the data reading program is 16. The initial learning rate is 1e-3. The learning rate dynamic adjustment strategy is ReduceLROnPlateau. The optimizer is AdamW [52]. The training epoch number is 100. Train with automatic mixed precision. The loss function is FocalLoss [53], which can reduce the weight of samples that are easy to classify and increase the weight of samples that are difficult to classify. Its formula is as follows:

$$FL(p_t) = -\alpha_t(1 - p_t)^\gamma \log(p_t) \quad (6)$$

$p \in [0,1]$ is the model's estimated probability of the labeled class, γ is an adjustable focusing parameter, and α is a balancing parameter. We set γ to 2 and α to 0.25.

C. Evaluation Metrics

In order to evaluate the performance and efficiency of the proposed LEDNet model, our evaluation indicators are divided into two categories. The first category is to evaluate the accuracy of the network, including Overall Accuracy (OA), average F1-Score (F1) and mean Intersection over Union (mIoU). The results of these evaluation indicators are calculated based on the confusion matrix, where TP indicates the number of True Positive categories, TN indicates the number of True Negative categories, FP indicates the number of False Positive categories, and FN indicates the number of False Negative categories.

Overall Accuracy (OA) is used to measure the overall accuracy of the model prediction results:

$$OA = \frac{TP + TN}{TP + TN + FP + FN} \quad (7)$$

The F1-Score (F1) indicates the comprehensive consideration of Precision and Recall:

$$Precision = \frac{TP}{TP + FP} \quad (8)$$

$$Precision = \frac{TP}{TP + FN} \quad (9)$$

$$F1 = 2 \frac{Precision \times Recall}{Precision + Recall} = \frac{2TP}{2TP + FP + FN} \quad (10)$$

Intersection over Union (IoU) is used to measure the ratio of the intersection and union of the predicted results of a certain category and the true value of the model:

$$IoU = \frac{TP}{TP + FN + FP} \quad (11)$$

The second category is to evaluate the scale of the network, including floating point operations (FLOPs) for evaluating complexity, frames per second (FPS) for evaluating speed, memory usage (MB) and the number of model parameters (M) to evaluate memory requirements.

D. Results on the Private dataset

In this part of the experiments, LEDNet is compared with some other semantic segmentation models on the constructed private dataset. These models include GCNet [36], PSPNet [5], SegFormer [54], and A2FPN [55], DC-Swin [56], BuildFormer [57] proposed for remote sensing semantic segmentation. The backbone network of other models is ResNet18, and LEDNet uses the proposed backbone network LEDNet. The comparison results are shown in Table I and Fig.5. It is clear that the proposed model far outperforms other models on the constructed private dataset. The mIoU of the proposed model is 4.59% higher than that of the powerful BuildFormer. In particular, its extraction rate for roads is also high.

TABLE IV
ABLATION STUDY

Dataset	Method	Overall Accuracy	Mean F1-Score	mIoU
LoveDA	Baseline	94.79	75.77	63.24
	Baseline + ASPP	95.21	76.14	63.79
	Baseline + OCR	95.29	77.02	64.79
	Baseline + ASPP + OCR	95.42	77.41	65.27
CITY_OSM	Baseline	90.19	84.82	73.70
	Baseline + ASPP	90.36	85.11	74.12
	Baseline + OCR	90.32	85.03	74.00
	Baseline + ASPP + OCR	90.49	85.28	74.39

E. Results on the public dataset "LoveDA"

In this part of the experiment, the same model as the above experiments and the proposed LEDCNet are used for comparison on the GG dataset "LoveDA". The comparison results are shown in Table II and Fig.6. Our model outperforms other models in both quantitative and qualitative results on the public dataset "LoveDA". The proposed model outperforms other models in both quantitative and qualitative results on the public dataset "LoveDA". Its mIoU is 1.22% higher than the powerful BuildFormer.

F. Results on the public dataset "CITY-OSM"

Consistent with the previous experiments, the public dataset selected in this part of the experiment is "CITY-OSM". On such a large-scale data set, the performance of the proposed basic model is slightly inferior to the two models of PSP-Net and BuildFormer. This demonstrates that the proposed basic model has good generalization ability on smaller scale datasets. Therefore, by adjusting the hyperparameters, the depth and size of the network are increased, and a larger model is obtained. Its performance outperforms other models.

G. Evaluation of Model Efficiency

It can be seen from the Table V that the proposed model, whether it is the basic version or the enlarged version, has smaller parameters and model sizes than other models. In addition, the FLOPs of the proposed basic version of the model is also the smallest. Therefore, the proposed model can be applied in a variety of hardware performance-limited scenarios. However, the proposed model still has shortcomings, that is, the FPS is not the highest, which is what we need to improve in the next step.

TABLE V
EVALUATION OF MODEL EFFICIENCY

Method	Params (M)	Size (MB)	FLOPs (G)	FPS
DC-Swin	118	237.858	126.15	34.7
SegFormer	7.7	15.436	13.11	115.2
GCNet	61.5	122.933	9.84	182.6
A2FPN	12.2	24.318	13.21	212.4
PSPNet	24.3	48.648	96.53	98.5
BuildFormer	40.5	81.038	116.22	52.4
LEDCNet (ours)	1.4	2.628	5.48	100.6
LEDCNet-large (ours)	<u>6.1</u>	<u>12.271</u>	13.69	52.0

H. Ablation study

In order to evaluate the contribution of each component of the proposed LEDCNet to the model performance. This study conducts ablation experiments on the model on the public datasets "LoveDA" and "CITY_OSM". The results are shown in the table III. After adding the ASPP module to the baseline model, its mIoU on the two public datasets increased by 0.55% and 0.42%, respectively. After adding the OCR module to the baseline model, its mIoU on the two public datasets increased by 1.55% and 0.88%, respectively. After the proposed model aggregates these two modules, its mIoU on two public datasets improves by 2.03% and 0.69% compared to the baseline model, respectively.

V. CONCLUSION

In this research, a lightweight and efficient network implemented using a dual-context module was developed for the extraction of ground features from UAV aerial remote sensing images. The proposed model is able to effectively capture multi-scale contextual information. It achieves high performance on both private and public datasets, and has a low amount of parameters and operations. In addition, this study designs a software platform for the proposed model, which facilitates the generalization and application of the proposed model. Moreover, the developed software has been approved by a Chinese government agency and put into actual production application.

REFERENCES

- [1] L. P. Osco, J. M. Junior, A. P. M. Ramos, L. A. de Castro Jorge, S. N. Fatholahi, J. de Andrade Silva, E. T. Matsubara, H. Pistori, W. N. Gonçalves, and J. Li, "A review on deep learning in uav remote sensing," *International Journal of Applied Earth Observation and Geoinformation*, vol. 102, p. 102456, 2021.
- [2] J. Long, E. Shelhamer, and T. Darrell, "Fully convolutional networks for semantic segmentation," in *Proceedings of the IEEE conference on computer vision and pattern recognition*, 2015, pp. 3431–3440.
- [3] V. Badrinarayanan, A. Kendall, and R. Cipolla, "Segnet: A deep convolutional encoder-decoder architecture for image segmentation," *IEEE transactions on pattern analysis and machine intelligence*, vol. 39, no. 12, pp. 2481–2495, 2017.
- [4] O. Ronneberger, P. Fischer, and T. Brox, "U-net: Convolutional networks for biomedical image segmentation," in *International Conference on Medical image computing and computer-assisted intervention*. Springer, 2015, pp. 234–241.
- [5] H. Zhao, J. Shi, X. Qi, X. Wang, and J. Jia, "Pyramid scene parsing network," in *Proceedings of the IEEE conference on computer vision and pattern recognition*, 2017, pp. 2881–2890.
- [6] L.-C. Chen, G. Papandreou, I. Kokkinos, K. Murphy, and A. L. Yuille, "Semantic image segmentation with deep convolutional nets and fully connected crfs," *arXiv preprint arXiv:1412.7062*, 2014.

- [7] —, “Deeplab: Semantic image segmentation with deep convolutional nets, atrous convolution, and fully connected crfs,” *IEEE transactions on pattern analysis and machine intelligence*, vol. 40, no. 4, pp. 834–848, 2017.
- [8] L.-C. Chen, G. Papandreou, F. Schroff, and H. Adam, “Rethinking atrous convolution for semantic image segmentation,” *arXiv preprint arXiv:1706.05587*, 2017.
- [9] L.-C. Chen, Y. Zhu, G. Papandreou, F. Schroff, and H. Adam, “Encoder-decoder with atrous separable convolution for semantic image segmentation,” in *Proceedings of the European conference on computer vision (ECCV)*, 2018, pp. 801–818.
- [10] Y. Yuan, X. Chen, X. Chen, and J. Wang, “Segmentation transformer: Object-contextual representations for semantic segmentation,” *arXiv preprint arXiv:1909.11065*, 2019.
- [11] T.-Y. Lin, P. Dollár, R. Girshick, K. He, B. Hariharan, and S. Belongie, “Feature pyramid networks for object detection,” in *Proceedings of the IEEE conference on computer vision and pattern recognition*, 2017, pp. 2117–2125.
- [12] G. Huang, Z. Liu, L. Van Der Maaten, and K. Q. Weinberger, “Densely connected convolutional networks,” in *Proceedings of the IEEE conference on computer vision and pattern recognition*, 2017, pp. 4700–4708.
- [13] Z. Liu, H. Mao, C.-Y. Wu, C. Feichtenhofer, T. Darrell, and S. Xie, “A convnet for the 2020s,” in *Proceedings of the IEEE/CVF Conference on Computer Vision and Pattern Recognition*, 2022, pp. 11 976–11 986.
- [14] Z. Liu, Y. Lin, Y. Cao, H. Hu, Y. Wei, Z. Zhang, S. Lin, and B. Guo, “Swin transformer: Hierarchical vision transformer using shifted windows,” in *Proceedings of the IEEE/CVF International Conference on Computer Vision*, 2021, pp. 10 012–10 022.
- [15] K. He, X. Zhang, S. Ren, and J. Sun, “Deep residual learning for image recognition,” in *Proceedings of the IEEE conference on computer vision and pattern recognition*, 2016, pp. 770–778.
- [16] E. Maggiori, Y. Tarabalka, G. Charpiat, and P. Alliez, “Convolutional neural networks for large-scale remote-sensing image classification,” *IEEE Transactions on geoscience and remote sensing*, vol. 55, no. 2, pp. 645–657, 2016.
- [17] Y. Liu, D. Minh Nguyen, N. Deligiannis, W. Ding, and A. Munteanu, “Hourglass-shapenetwork based semantic segmentation for high resolution aerial imagery,” *Remote Sensing*, vol. 9, no. 6, p. 522, 2017.
- [18] G. Fu, C. Liu, R. Zhou, T. Sun, and Q. Zhang, “Classification for high resolution remote sensing imagery using a fully convolutional network,” *Remote Sensing*, vol. 9, no. 5, p. 498, 2017.
- [19] R. Li, W. Liu, L. Yang, S. Sun, W. Hu, F. Zhang, and W. Li, “Deepunet: A deep fully convolutional network for pixel-level sea-land segmentation,” *IEEE Journal of Selected Topics in Applied Earth Observations and Remote Sensing*, vol. 11, no. 11, pp. 3954–3962, 2018.
- [20] B. Cheng, C. Liang, X. Liu, Y. Liu, X. Ma, and G. Wang, “Research on a novel extraction method using deep learning based on gf-2 images for aquaculture areas,” *International Journal of Remote Sensing*, vol. 41, no. 9, pp. 3575–3591, 2020.
- [21] Y. Wang, Y. Peng, W. Li, G. C. Alexandropoulos, J. Yu, D. Ge, and W. Xiang, “Ddu-net: dual-decoder-u-net for road extraction using high-resolution remote sensing images,” *IEEE Transactions on Geoscience and Remote Sensing*, vol. 60, pp. 1–12, 2022.
- [22] S. Song, J. Liu, Y. Liu, G. Feng, H. Han, Y. Yao, and M. Du, “Intelligent object recognition of urban water bodies based on deep learning for multi-source and multi-temporal high spatial resolution remote sensing imagery,” *Sensors*, vol. 20, no. 2, p. 397, 2020.
- [23] L. Weng, Y. Xu, M. Xia, Y. Zhang, J. Liu, and Y. Xu, “Water areas segmentation from remote sensing images using a separable residual segnet network,” *ISPRS International Journal of Geo-Information*, vol. 9, no. 4, p. 256, 2020.
- [24] V. V. Kniaz, “Deep learning for dense labeling of hydrographic regions in very high resolution imagery,” in *Image and signal processing for remote sensing XXV*, vol. 11155. SPIE, 2019, pp. 283–292.
- [25] I. Goodfellow, J. Pouget-Abadie, M. Mirza, B. Xu, D. Warde-Farley, S. Ozair, A. Courville, and Y. Bengio, “Generative adversarial networks,” *Communications of the ACM*, vol. 63, no. 11, pp. 139–144, 2020.
- [26] Q. Wang, H. Huang, Y. Zhong, W. Min, Q. Han, D. Xu, and C. Xu, “Swin transformer based on two-fold loss and background adaptation re-ranking for person re-identification,” *Electronics*, vol. 11, no. 13, p. 1941, 2022.
- [27] R. Li, S. Zheng, C. Zhang, C. Duan, J. Su, L. Wang, and P. M. Atkinson, “Multiattention network for semantic segmentation of fine-resolution remote sensing images,” *IEEE Transactions on Geoscience and Remote Sensing*, vol. 60, pp. 1–13, 2021.
- [28] C. Zhang, W. Jiang, Y. Zhang, W. Wang, Q. Zhao, and C. Wang, “Transformer and cnn hybrid deep neural network for semantic segmentation of very-high-resolution remote sensing imagery,” *IEEE Transactions on Geoscience and Remote Sensing*, vol. 60, pp. 1–20, 2022.
- [29] A. G. Howard, M. Zhu, B. Chen, D. Kalenichenko, W. Wang, T. Weyand, M. Andreetto, and H. Adam, “Mobilenets: Efficient convolutional neural networks for mobile vision applications,” *arXiv preprint arXiv:1704.04861*, 2017.
- [30] M. Sandler, A. Howard, M. Zhu, A. Zhmoginov, and L.-C. Chen, “Mobilenetv2: Inverted residuals and linear bottlenecks,” in *Proceedings of the IEEE conference on computer vision and pattern recognition*, 2018, pp. 4510–4520.
- [31] A. Howard, M. Sandler, G. Chu, L.-C. Chen, B. Chen, M. Tan, W. Wang, Y. Zhu, R. Pang, V. Vasudevan *et al.*, “Searching for mobilenetv3,” in *Proceedings of the IEEE/CVF international conference on computer vision*, 2019, pp. 1314–1324.
- [32] F. N. Iandola, S. Han, M. W. Moskewicz, K. Ashraf, W. J. Dally, and K. Keutzer, “Squeezenet: Alexnet-level accuracy with 50x fewer parameters and 0.5 mb model size,” *arXiv preprint arXiv:1602.07360*, 2016.
- [33] M. Tan and Q. Le, “Efficientnet: Rethinking model scaling for convolutional neural networks,” in *International conference on machine learning*. PMLR, 2019, pp. 6105–6114.
- [34] K. Han, Y. Wang, Q. Tian, J. Guo, C. Xu, and C. Xu, “Ghostnet: More features from cheap operations,” in *Proceedings of the IEEE/CVF conference on computer vision and pattern recognition*, 2020, pp. 1580–1589.
- [35] Y. Li, Y. Chen, X. Dai, D. Chen, M. Liu, L. Yuan, Z. Liu, L. Zhang, and N. Vasconcelos, “Micronet: Improving image recognition with extremely low flops,” in *Proceedings of the IEEE/CVF International Conference on Computer Vision*, 2021, pp. 468–477.
- [36] Y. Cao, J. Xu, S. Lin, F. Wei, and H. Hu, “Gcnet: Non-local networks meet squeeze-excitation networks and beyond,” in *Proceedings of the IEEE/CVF international conference on computer vision workshops*, 2019, pp. 0–0.
- [37] C. Peng, X. Zhang, G. Yu, G. Luo, and J. Sun, “Large kernel matters—improve semantic segmentation by global convolutional network,” in *Proceedings of the IEEE conference on computer vision and pattern recognition*, 2017, pp. 4353–4361.
- [38] S. Xie, R. Girshick, P. Dollár, Z. Tu, and K. He, “Aggregated residual transformations for deep neural networks,” in *Proceedings of the IEEE conference on computer vision and pattern recognition*, 2017, pp. 1492–1500.
- [39] I. Radosavovic, J. Johnson, S. Xie, W.-Y. Lo, and P. Dollár, “On network design spaces for visual recognition,” in *Proceedings of the IEEE/CVF international conference on computer vision*, 2019, pp. 1882–1890.
- [40] I. Radosavovic, R. P. Kosaraju, R. Girshick, K. He, and P. Dollár, “Designing network design spaces,” in *Proceedings of the IEEE/CVF conference on computer vision and pattern recognition*, 2020, pp. 10 428–10 436.
- [41] C. Szegedy, W. Liu, Y. Jia, P. Sermanet, S. Reed, D. Anguelov, D. Erhan, V. Vanhoucke, and A. Rabinovich, “Going deeper with convolutions,” in *Proceedings of the IEEE conference on computer vision and pattern recognition*, 2015, pp. 1–9.
- [42] A. Krizhevsky, I. Sutskever, and G. E. Hinton, “Imagenet classification with deep convolutional neural networks,” *Communications of the ACM*, vol. 60, no. 6, pp. 84–90, 2017.
- [43] K. Simonyan and A. Zisserman, “Very deep convolutional networks for large-scale image recognition,” *arXiv preprint arXiv:1409.1556*, 2014.
- [44] A. Lavin and S. Gray, “Fast algorithms for convolutional neural networks,” in *Proceedings of the IEEE conference on computer vision and pattern recognition*, 2016, pp. 4013–4021.
- [45] X. Ding, X. Zhang, J. Han, and G. Ding, “Scaling up your kernels to 31x31: Revisiting large kernel design in cnns,” in *Proceedings of the IEEE/CVF Conference on Computer Vision and Pattern Recognition*, 2022, pp. 11 963–11 975.
- [46] M.-H. Guo, C.-Z. Lu, Z.-N. Liu, M.-M. Cheng, and S.-M. Hu, “Visual attention network,” *arXiv preprint arXiv:2202.09741*, 2022.
- [47] S. Ioffe, “Batch renormalization: Towards reducing minibatch dependence in batch-normalized models,” *Advances in neural information processing systems*, vol. 30, 2017.
- [48] Y. Wu and J. Johnson, “Rethinking” batch” in batchnorm,” *arXiv preprint arXiv:2105.07576*, 2021.
- [49] J. L. Ba, J. R. Kiros, and G. E. Hinton, “Layer normalization,” *arXiv preprint arXiv:1607.06450*, 2016.
- [50] J. Wang, Z. Zheng, A. Ma, X. Lu, and Y. Zhong, “Loveda: A remote sensing land-cover dataset for domain adaptive semantic segmentation,” *arXiv preprint arXiv:2110.08733*, 2021.

- [51] P. Kaiser, J. D. Wegner, A. Lucchi, M. Jaggi, T. Hofmann, and K. Schindler, "Learning aerial image segmentation from online maps," *IEEE Transactions on Geoscience and Remote Sensing*, vol. 55, no. 11, pp. 6054–6068, 2017.
- [52] I. Loshchilov and F. Hutter, "Fixing weight decay regularization in adam," 2018.
- [53] T.-Y. Lin, P. Goyal, R. Girshick, K. He, and P. Dollár, "Focal loss for dense object detection," in *Proceedings of the IEEE international conference on computer vision*, 2017, pp. 2980–2988.
- [54] E. Xie, W. Wang, Z. Yu, A. Anandkumar, J. M. Alvarez, and P. Luo, "Segformer: Simple and efficient design for semantic segmentation with transformers," *Advances in Neural Information Processing Systems*, vol. 34, pp. 12 077–12 090, 2021.
- [55] R. Li, L. Wang, C. Zhang, C. Duan, and S. Zheng, "A2-fpn for semantic segmentation of fine-resolution remotely sensed images," *International journal of remote sensing*, vol. 43, no. 3, pp. 1131–1155, 2022.
- [56] L. Wang, R. Li, C. Duan, C. Zhang, X. Meng, and S. Fang, "A novel transformer based semantic segmentation scheme for fine-resolution remote sensing images," *IEEE Geoscience and Remote Sensing Letters*, vol. 19, pp. 1–5, 2022.
- [57] L. Wang, S. Fang, X. Meng, and R. Li, "Building extraction with vision transformer," *IEEE Transactions on Geoscience and Remote Sensing*, vol. 60, pp. 1–11, 2022.

VI. BIOGRAPHY SECTION



Xiaoxiang Han is currently pursuing the master degree in the School of Health Science and Engineering, University of Shanghai for Science and Technology.

His research interests include deep learning, computer vision, medical image processing, remote sensing image processing, unsupervised algorithms, etc.



Yiman Liu received the B.E. degree in medical imaging engineering from the University of Shanghai for Science and Technology of China, Shanghai, China, in 2015.

In 2015, he joined the Department of Pediatric Cardiology, Shanghai Children's Medical Center, School of Medicine, Shanghai Jiao Tong University, Shanghai, China. Mainly engaged in pediatric cardiac ultrasound diagnosis.

He is currently pursuing the master's degree in electronics and communication engineering with

East China Normal University, Shanghai. His current research interests include deep learning, computer vision, Natural Language Processing, and artificial intelligence for medical image analysis.



Gang Liu was born in August 1984, associate researcher. In 2018, he graduated from China University of Geosciences (Wuhan), majoring in geophysics, and received a doctorate in science. In 2011, he worked in Hubei Earthquake Administration (Seismological Research Institute of China Earthquake Administration), and was named as an associate researcher in 2017. In 2020, he was selected as a "Youth Talent" of China Earthquake Administration.

He is mainly engaged in the research of seismic geodesy, including: the application of high-frequency GNSS in seismology; the study of the physical process of the source by comprehensive observation methods; the deformation characteristics and simulation research of the earthquake cycle; the current deformation characteristics and stress evolution process of active faults. Focus on using joint inversion to constrain the source parameters and rupture process of large earthquakes.



Qiaohong Liu was born in Hubei, China, in 1979. She received the B.S. degree in engineering from the Wuhan University of Technology, in 2001, the M.S. degree in science from the Huazhong University of Science and Technology, in 2004, and the Ph.D. degree in control theory and control engineering from Shanghai University, in 2015. She is currently a Lecturer with the Shanghai University of Medicine and Health Sciences. She has authored more than 20 journal papers and has written two book chapters.

Her current research interests include image deblurring, image denoising, and computer vision.